Characterization of an Anisotropic Hydrogel Tissue Substrate for Infusion Testing

Sung Jin Lee,[1] Gregory L. Pishko,[1] Garret W. Astary,[2] Thomas H. Mareci,[3] Malisa Sarntinoranont[1]

[1]*Department of Mechanical and Aerospace Engineering, University of Florida, Gainesville, FL 32611*
[2]*Department of Biomedical Engineering, University of Florida, Gainesville, FL 32611*
[3]*Department of Biochemistry and Molecular Biology, University of Florida, Gainesville, FL 32611*

Received 9 December 2008; accepted 18 April 2009
DOI 10.1002/app.30639
Published online 30 June 2009 in Wiley InterScience (www.interscience.wiley.com).

ABSTRACT: Artificial tissue models that capture specific transport properties are useful for investigating physical phenomena important to drug delivery. In this study, an *in vitro* tissue model was developed and characterized with the goal of mimicking aligned tissue. An anisotropic porous medium was developed by the construction of a 1% agarose hydrogel implanted with different volume fractions ($\sim$ 5, 10, and 20%) of 10-μm-diameter glass fibers. The developed substrate was able to capture anisotropic transport after the direct infusion of a macromolecular tracer, Evans blue albumin (EBA). To further characterize the test substrate, the diffusion tensor of water was measured by diffusion tensor imaging, and the ratios of the diffusivities in the directions parallel and perpendicular to the glass fibers were 1.16, 1.20, and 1.26 for 5, 10, and 20% fiber volume fractions, respectively. The hydraulic conductivity was estimated by the measurement of pressure gradients across samples under controlled microflow conditions in the direction parallel to implanted fibers. The hydraulic conductivities at various hydrogel concentrations without fibers and in a 1% hydrogel with various fiber volume fractions were measured; for example, $K_{\parallel} = 1.20 \times 10^{-12}$ m^4 N^{-1} s^{-1} (where $K_{\parallel}$ is the conductivity component in the direction parallel to the glass fibers) for 20% fiber volume fractions. Also, EBA distributions were fit to porous medium transport models to estimate hydraulic conductivity in the direction perpendicular to glass fibers. The estimated ratio of directional hydraulic conductivity, $K_{\parallel}/K_{\perp}$ (where $K_{\perp}$ is the conductivity component in the direction perpendicular to the glass fibers), ranged from approximately 3 to 5, from 6 to 10, and from 40 to 90 for 5, 10, and 20% fiber volume fractions, respectively. These agarose hydrogel models provided convenient media for quantifying infusion protocols at low flow rates. © 2009 Wiley Periodicals, Inc. J Appl Polym Sci 114: 1992–2002, 2009

Key words: bioengineering; biopolymers; diffusion; drug delivery systems; hydrogels

INTRODUCTION

In tissue engineering and drug delivery, agarose hydrogels are popular because they have macromolecular properties similar to those of natural extracellular matrix,[1,2] are easy to fabricate, and are mechanically stable.[3] These hydrogels have a porous structure characterized by isotropic transport. However, the addition of longitudinally oriented fibers to hydrogels can create an anisotropic structure. Through the development of such fiber-embedded hydrogels, the goal of this study was to develop a spinal cord tissue surrogate incorporating anisotropic transport as an intrinsic material property. Specifically, extracellular transport in the spinal cord has been shown to be anisotropic with preferential transport in the direction parallel to axonal fibers.[4–6]

Isotropic transport properties in agarose gels have been previously measured. Tao and Nicholson[7] measured the diffusivity of bovine serum albumin (BSA) in agarose gels using integrative optical imaging analysis. The diffusivity was $8.29 \pm 0.17 \times 10^{-7}$ cm^2/s for 0.6% gels formed with physiological saline at 34°C. Liang et al.[8] measured the diffusivity of BSA in agarose gels using a refractive index method, and the measured diffusivity ranged from 4.98 to 8.21×10^{-7} cm^2/s for various agarose concentrations (0.5–3.0 wt %) formed in distilled water.[8] Hydraulic conductivity, which is a measure of the conductance to fluid flow under a pressure gradient, has also been measured in agarose gels by the measurement of the fluid filtration rate and by confined compression testing. Measured values for 2% agarose gels range from 3.53 to 6.61×10^{-13} m^4 N^{-1} s^{-1}.[9–11] A biphasic analysis of dynamic responses from confined compression tests has also shown this property to be deformation-dependent in agarose gels.[11]

Correspondence to: M. Sarntinoranont (msarnt@ufl.edu).
Contract grant sponsor: National Institutes of Health; contract grant number: R21 NS052670.

Several approaches to fabricating anisotropic hydrogels, including electrospinning, dielectrophoretic assembly, and strong magnetic fields, have been developed.[12–16] In this study, glass fibers were embedded in an agarose hydrogel to create an anisotropic structure. This construct was chosen on account of the inert properties of the fibers and ease of manufacture because specialized equipment was not required. In a related study, Gillies et al.[17] developed a spinal cord surrogate model using 0.6% agarose gel and 8-μm-diameter glass fibers at a volume fraction of the order of 10%. Their tissue surrogate was successfully shown to capture anisotropic transport after the infusion of a low-molecular-weight dye. They measured the ratio of the longitudinal mass flow to the transverse mass flow; however, more extensive transport characterization was not undertaken. For example, measurement of the directional hydraulic conductivities would be useful in analyzing the anisotropic transport of arbitrary compounds.

In this study, a similar tissue surrogate was developed with a 1.0% agarose hydrogel and 10-μm-diameter glass fibers with volume fractions ranging from 5 to 20%. The 10-μm glass fibers were initially chosen for these preliminary tests because they provide a microscale structure that is on the same length scale as neuronal axonal fibers. Without fibers, agarose hydrogels are isotropic in their porous structure. However, with the inclusion of dispersed and uniformly oriented glass fibers, transport in the direction perpendicular to fiber alignment is hindered, and transport in this plane is reduced. However, transport in the hydrogel space parallel to the glass fibers is less hindered, and this leads to preferential transport in this direction. The anisotropic transport properties of developed tissue substrates were extensively characterized with (1) noninvasive magnetic resonance (MR) imaging techniques to measure the effective diffusion tensor of water, (2) permeameter tests to measure hydraulic conductivity, and (3) tracer distribution studies that determined the ratio of directional hydraulic conductivities. Such agarose-hydrogel-based models provide convenient media for quantifying tissue infusion protocols. We expect that the developed hydrogel model could be used as a test bed medium for *in vitro* transport studies in the spinal cord or other tissues with intrinsic anisotropic transport properties.

EXPERIMENTAL

Sample preparation

Glass fibers (10 μm in diameter) were cut to a length of 20 mm and placed in a glass tube container with a 4.2-mm inner diameter, filling 5, 10, or 20% of the tube volume. To minimize the volume of air bubbles within the final sample, the following protocol was adopted. The samples were submerged under water and heated at 60°C for approximately 3 h, they were allowed to cool at room temperature, and then any air bubbles that formed were eliminated with a vacuum pump. An agarose based hydrogel, Trevigel 5000 (Trevigen, Gaithersburg, MD), was used to form the homogeneous gel structure. Transport properties were measured in hydrogels with and without fibers. For samples without fibers, hydrogel powders at concentrations of 0.5, 0.75, 1, and 1.5% (w/v) were dissolved and heated in deionized water. For samples with embedded fibers, a 1% (w/v) agarose hydrogel was used with various volume fractions of glass fibers. Next, the glass tube containing the hydrated glass-fiber bundle was submerged vertically in the hydrogel solution, and tweezers were used to mix and distribute the fibers evenly. Because of the relative stiffness and short length of the fibers, the glass fibers stayed relatively straight within the glass tubes. Finally, samples were cooled to room temperature over approximately 2 h and stored at 4°C until testing. The aligned microstructure of a sample specimen with a 20% fiber volume fraction after freezing and dissection is shown in Figure 1.

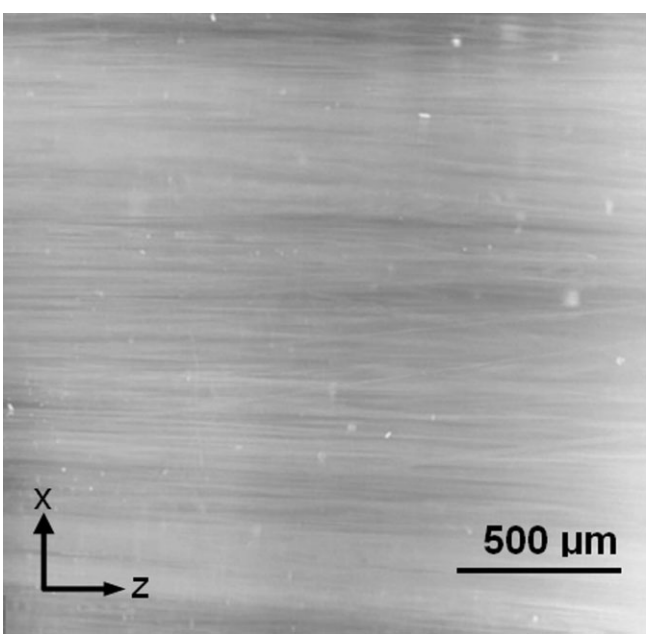

Figure 1 Structure of the glass-fiber/hydrogel construct (20% glass-fiber volume in a 1% agarose hydrogel) captured by microscopy after the freezing and dissection of the sample.

High-resolution MR imaging and diffusion tensor imaging (DTI)

MR images of hydrogel samples embedded with glass fibers at a concentration of 0, 5, 10, or 20% (one sample each) were captured at 19°C with a 14.1-T (at 600 MHz) MR imaging spectrometer (Bruker NMR Instruments, Billeria, MA). High-resolution images were measured with a three-dimensional gradient echo sequence with a recovery time of 150 ms and an echo time of 10 ms with four signal averages. The field of view was 10 mm × 5 mm × 5 mm in a matrix of 256 × 128 × 128. Diffusion-weighted images were measured with a multiple-slice, spin-echo sequence with a recovery time of 1400 ms and an echo time of 28 ms with four signal averages. The field of view was 4.2 mm × 4.2 mm in a matrix of 70 × 70 with 12 slices 0.3 mm thick. A total of 27 diffusion-weighted images were measured: 6 images with low diffusion weighting (98 s/mm^2) and 21 with high diffusion weighting (1240 s/mm^2). The diffusion weighting directions were equally distributed over a unit hemisphere. Custom software, written in the interactive data language (Research Systems, Inc., Boulder, CO), was used to process the image data. The spatially encoded data were Fourier-transformed to produce both high-resolution images and diffusion-weighted images. Then, diffusion-weighted images were interpolated (bilinear interpolation with nearest neighbor sampling) by a factor of 2 in each dimension. After the initial image processing, the multiple-slice, diffusion-weighted image data were fit to a rank-2 tensor model of water translational diffusion (D_e) with multiple linear regression.[18] Because of the alignment of the sample with the measured coordinate system (the z direction is parallel to the glass fibers), the effective diffusion tensor can be expressed as follows:

$$\mathbf{D}_{eij} = \begin{bmatrix} \lambda_x & 0 & 0 \\ 0 & \lambda_y & 0 \\ 0 & 0 & \lambda_z \end{bmatrix} \quad (1)$$

where λ_x, λ_y, and λ_z are the diffusivity eigenvalues. The anisotropy of translational diffusion is characterized by the fractional anisotropy (FA), which increases in magnitude with increasing diffusion anisotropy:

$$\mathrm{FA} = \sqrt{\frac{3}{2}} \frac{\sqrt{(\lambda_x - \overline{D})^2 + (\lambda_y - \overline{D})^2 + (\lambda_z - \overline{D})^2}}{\sqrt{\lambda_x^2 + \lambda_y^2 + \lambda_z^2}}, \quad (2)$$

where $\overline{D}$ is the mean diffusivity. $\overline{D}$ was calculated with $\overline{D} = Tr(D_e)/3$. Both D_e and FA were calculated on a voxel-by-voxel basis.

Hydraulic conductivity tests

Hydraulic conductivity was measured with a one-dimensional flow-controlled permeameter system. Hydrogel samples with and without glass fibers were tested. The first test group with no glass fibers included 0.5, 0.75, 1, and 1.5% agarose hydrogel concentrations. Samples with no fibers were tested to determine the ideal hydrogel percentage for fibers with respect to fabrication and infusion issues. Also, we were interested in establishing baseline values for the hydraulic conductivity of the agarose hydrogel for comparison with the measured values in hydrogel–fiber composites. For each hydrogel concentration, five samples were tested. In these tests, the low-concentration hydrogels (0.5%) were difficult to use because of their softness, whereas higher concentration (2%) hydrogels were stiffer and more prone to damage with cannula insertion (e.g., infusate backflow along the cannula). The 1% concentration provided good mechanical properties for handling, and this concentration was used in all glass-fiber infusion studies. In the second group, glass fibers at concentrations of 5, 10, and 20% (v/v) were embedded in 1% agarose hydrogels. For each fiber volume fraction, four samples were tested.

For these tests, hydrogel samples were surrounded by an acrylic tube (4-mm inner diameter and 10-mm length). The permeameter consisted of a syringe pump (model 100, KD Scientific, Holliston, MA), a syringe connected to a hydrogel holder with noncompliant poly(ether ether ketone) tubing, brass fittings (Swagelok, Solon, OH), and a pressure transducer (Fig. 2). To eliminate air bubbles, the system was assembled while submerged in deionized water. The syringe pump drove deionized water from a 250-μL gas-tight syringe (Hamilton, Reno, NV)

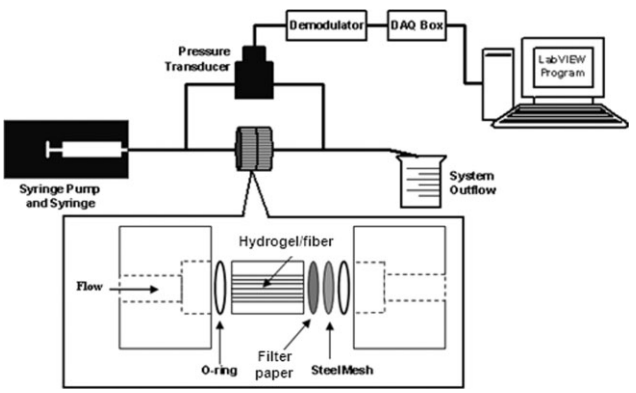

Figure 2 Experimental setup for the measurement of the hydraulic conductivity in the agarose hydrogel samples. The pressure drop was measured across samples subject to a constant flow rate. For samples with fibers, the fiber alignment was in the direction parallel to the flow through the sample.

through the hydrogel sample at constant flow rates of 10–50 μL/h. Filter paper and a wire mesh provided mechanical support for the hydrogel sample. A variable-reluctance differential pressure transducer (DP15-32, Validyne, Northridge, CA) was connected upstream and downstream of the hydrogel holder to measure the pressure difference across the sample. Output signals were sent to a demodulator (CD280-4, Validyne) for amplification and to a data acquisition (DAQ) box for input into LabVIEW Express, version 7 (National Instruments, Austin, TX), which converted the voltage signal to a pressure reading. The transducer was calibrated by being connected to a set of differential height water columns, which were varied from 0 to 14.7 kPa (150 cm H_2O). A linear relationship was determined between the voltage and pressure. Also, the pressure drop due to the tubing, fittings, filter paper, and mesh support was found to be negligible ($<\pm 0.035$ kPa).

The steady-state pressure drop (ΔP) across the hydrogel samples was measured between 40 and 80 min after the initiation of flow once pressure variations were less than 1% over a 10-min period. ΔP was used to calculate the apparent hydraulic conductivity (K) at each flow rate with Darcy's law:

$$K = \frac{V \cdot L}{\Delta P} \tag{3}$$

where V is the volume-averaged fluid velocity and L is the length of the sample.

Tracer infusion tests

BSA (A-7284, Sigma, St. Louis, MO), which had a molecular weight of approximately 66,120 g/mol, was combined with Evans blue (E2129-10G, Sigma) in a 1 : 1 molar ratio. Evans blue albumin (EBA; 2.5% v/v) was diluted with deionized water and stored in a refrigerator (~ 5°C) until testing. A small albumin percentage was used to minimize osmotic effects in the hydrogel.

For hydrogel infusions, a 100-μL gas-tight syringe (Hamilton) was used with the syringe pump (Fig. 3), and a low infusion rate of 10 μL/h was chosen to minimize backflow. The syringe was coupled to a 32-gauge syringe needle (0.25-mm outer diameter), which was inserted via a guide cannula into the center of the hydrogel samples. A small-diameter needle was also used to reduce backflow and the damage due to insertion. Fluorescent light was used to backlight transparent hydrogels, and images of tracer distributions were taken with a single-lens reflex camera (D-50, Nikon, Tokyo, Japan). Tracer distributions were measured in 5-min intervals for a total of 20 min. Infused tracer images were converted to gray scale, and pixel intensities were converted to tracer concentrations. Because of the opaqueness of the glass-embedded samples, these samples were frozen in liquid nitrogen at select time points, dissected through the point of infusion, and photographed.

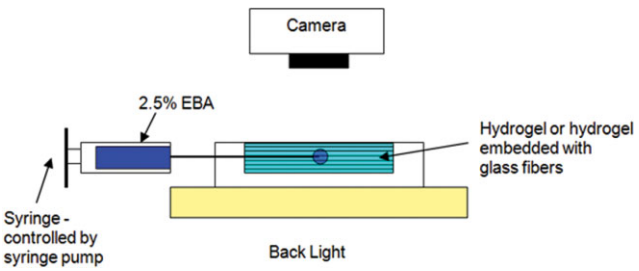

Figure 3 Experimental setup for the tracer infusion tests. [Color figure can be viewed in the online issue, which is available at www.interscience.wiley.com.]

Tracer distribution anisotropy was quantified by the measurement of the ellipse ratio, the a/b ratio of the tracer distribution lengths in the directions parallel (a) and perpendicular (b) to the glass fibers. With freezing, there were nonuniform volume changes in the hydrogel and glass fibers (i.e., there was a volume change of approximately 9% in the water phase, whereas the thermal shrinkage of glass was smaller). However, the tracer was confined to the hydrogel phase only. Thus, with freezing, the ellipse ratio within the hydrogel could be conserved with isotropic expansion of this phase. However, shrinkage in the direction perpendicular to the glass fibers could be hindered, and this would result in some underestimation of the ellipse ratio with freezing.

Porous medium transport model

The hydrogel was modeled as a rigid porous medium,[19] and the two-dimensional axisymmetric infusion problem was solved with Femlab 3.2 (Comsol, Inc., Burlington, MA). The main assumption of this model is that the pore space filled by a fluid is not deforming. This is a valid assumption if the polymer matrix of the hydrogel is not susceptible to deformation in the range of infusion pressures tested. Darcy's law and the continuity equation were solved under steady-state conditions to get the pressure (p) and velocity field surrounding the infusion point:

$$\mathbf{K}\nabla^2 p = 0 \tag{4}$$

where

$$\mathbf{K} = \begin{bmatrix} K_{\parallel} & 0 \\ 0 & K_{\perp} \end{bmatrix}$$

$\mathbf{K}$ is the hydraulic conductivity tensor, $K_{\parallel}$ is the conductivity component in the direction parallel to the

glass fibers, and $K_\perp$ is the conductivity component in the perpendicular plane. The prescribed boundary conditions were $\Delta p \times \mathbf{n} = 0$, where $\mathbf{n}$ is the unit normal vector along the symmetric and no-flux surfaces; $p = 0$ along cut ends; and a fixed pressure corresponding to 10 μL/h along the infusion site boundary.

The unsteady transport equation governing the EBA tracer concentration (C) was

$$\frac{\partial C}{\partial t} + \nabla \cdot (-\boldsymbol{D}\nabla C) = -\frac{u}{\phi} \cdot \nabla C \tag{5}$$

where

$$\boldsymbol{D} = \begin{bmatrix} D_\parallel & 0 \\ 0 & D_\perp \end{bmatrix}$$

u is the volume-averaged velocity, ϕ is the porosity or fluid volume fraction, and $\boldsymbol{D}$ is the diffusion tensor for the EBA tracer in the hydrogel. $D_\parallel$ is the diffusion component in the direction parallel to the glass fibers, and $D_\perp$ is the diffusion component in the perpendicular plane. In the pure hydrogel, which is isotropic, $D_\parallel = D_\perp = \boldsymbol{D}$. The prescribed boundary condition was $\nabla C \times \mathbf{n} = 0$ along axisymmetric and no-flux surfaces, $C = 0$ along cut ends, and $C/C_o = 1$ (with a normalized concentration, where C_o is the maximum concentration) along the infusion site boundary.

Diffusivity of EBA

Tracer diffusivity was estimated through an analysis of EBA infusion distributions in fiber-free hydrogels. Numerical simulations for porous medium transport were performed for a range of EBA tracer diffusivities, 4.0–9 $\times$ 10^{-7} cm^2/s, in intervals of 1.0 $\times$ 10^{-7} and for a range of ϕ values, 0.4–0.9, in intervals of 0.1. The range of $\boldsymbol{D}$ was selected to cover a physically relevant range. The high value of 9 $\times$ 10^{-7} cm^2/s is equivalent to BSA diffusivity in water, and the low value is bounded by BSA diffusivity measured in a higher (3%) concentration of agarose gel.[8] The increment of 10^{-7} cm^2/s was considered sufficient because predicted concentration profiles were not very sensitive to smaller increments. ϕ ranges were based on previous hydrogel infusion studies.[20] Tracer distribution images represented the integrated concentration through the hydrogel samples. Therefore, the numerical concentration solutions were integrated over the thickness of the hydrogels. These integrated concentration profiles were compared to the image data collected. Some concentration variations in the vicinity of the infusion cannula were induced by the formation of a local infusion cavity, hydrogel damage due to cannula insertion, or backflow. Because porous medium tracer simulations did not model these effects, experimental and numerical distribution data were compared at a set distance from the infusion point ($r/a > 1.0$, where r is the radial coordinate and a is the outer diameter of the syringe needle). Fifty spatial points along normalized concentration profiles at four time points (5, 10, 15, and 20 min) were compared with numerical simulations. Optimal values for $\boldsymbol{D}$ and ϕ were estimated by minimization of the mean square error (MSE) function:

$$\mathrm{MSE} = \frac{1}{m}\sum_{i=1}^{m}\sum_{j=1}^{n}(X_j^{Ei} - X_j^{ci})^2/q \tag{6}$$

where m is the total number of time points ($m = 4$); q is the total number of points along a concentration profile ($q = 50$); and X_j^{Ei} and X_j^{Ci} are the experimental and computational integrated concentration values, respectively.

$K_\perp$

$K_\parallel/K_\perp$ was estimated by an analysis of EBA distributions after infusion into 5, 10, and 20% fiber-embedded hydrogels. In numerical simulations using the porous medium transport model, the estimated ratio of water diffusivity from DTI was used to estimate the ratio of EBA diffusivities: $\lambda_z/\lambda_x = D_\parallel/D_\perp$. $D_\parallel$ was set to the value measured in the fiber-free hydrogel. $K_\parallel$ was set to the value measured in hydraulic conductivity tests. $K_\parallel/K_\perp$ was estimated to range from 20 to 200. The tracer ellipse from porous medium predictions was directly compared with measured EBA ellipse ratios. $K_\parallel/K_\perp$ was estimated within a range of ± 1 standard deviation (SD) of measured EBA ellipse ratios for each fiber volume fraction. In these comparisons, a threshold value of $C/C_o = 0.05$ was used to calculate the distribution contours.

RESULTS

High-resolution MR images and DTI

High-resolution MR images of the tissue surrogate (Fig. 4) clearly indicate regions of hydrogel (white), glass fibers (gray), and air bubbles (dark spots). The dark spots can be classified as air bubbles because they display the characteristic susceptibility artifact of air in an MR image.[21] The apparent size of air bubbles in the central regions of infusion was approximately 17 μm; however, the actual size was smaller because of the boundary effects of magnetic susceptibility between air and water. These microscopic air bubbles were not expected to significantly affect macromolecular transport. Diffusion tensor

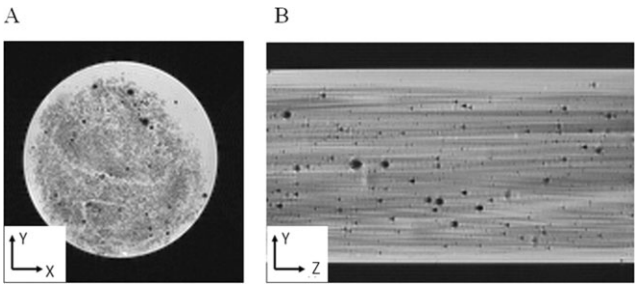

Figure 4 High-resolution MR images of the fabricated tissue surrogate (20% glass-fiber volume in a 1% agarose hydrogel) clearly showing the aligned glass-fiber structure. The transverse image (left) had a 5 × 5 mm^2 field of view, whereas the axial image (right) had a 5 × 7.6 mm^2 field of view (truncated for display). The black dots correspond to microscopic air bubbles. The voxel resolution was 40 × 40 × 40 μm^3.

images along with derived two-dimensional parametric maps are presented in Figure 5 for a glass-fiber/agarose-hydrogel sample (20% fiber volume fraction). These images show clear diffusional anisotropy with maximum diffusion in the z direction of fiber alignment.

Effective diffusivities of water in 1% hydrogel samples are presented in Table I for various fiber volume fractions. Water diffusivities in the fiber-free hydrogels were nearly isotropic and homogeneous with $\lambda_z/\lambda_\perp = 1.1$ and FA = 0.065 ± 0.017. With increasing glass-fiber content, water diffusivity in the plane perpendicular to the aligned fibers (x and y) decreased, and anisotropy measures, $\lambda_z/\lambda_\perp$ and FA, were found to increase. In the 20% volume fraction sample, FA was 0.15 ± 0.002, which was larger than that for fiber-free samples ($FA_{20\%fiber}/FA_{fiber\text{-}free} = 2.34$). Local diffusivity measures within a region of interest (ROI) were also compared with average values calculated over the entire sample. FA measured within high-fiber-density regions [circled regions within Fig. 5(A,B)] was approximately 10 to 30% higher than that over the entire sample. This variation indicates some spatial nonuniformity in the fiber distribution.

Hydraulic conductivity testing

In fiber-free samples, K varied with the agarose hydrogel concentration, that is, the volume fraction of water (Fig. 6). K decreased more than 10-fold as the concentration increased from 0.5 to 1.5%. (Note that data from previous hydrogel studies are plotted for reference.) Measured K values are listed in Table II, and K was 1.47 ± 0.3 × 10^{-12} m^4 N^{-1} s^{-1} for 1.0% hydrogels.

The effect of glass-fiber inclusion on hydrogel hydraulic conductivity was also measured at low average velocities (0.2–1.1 × 10^{-6} m/s). For both fiber-

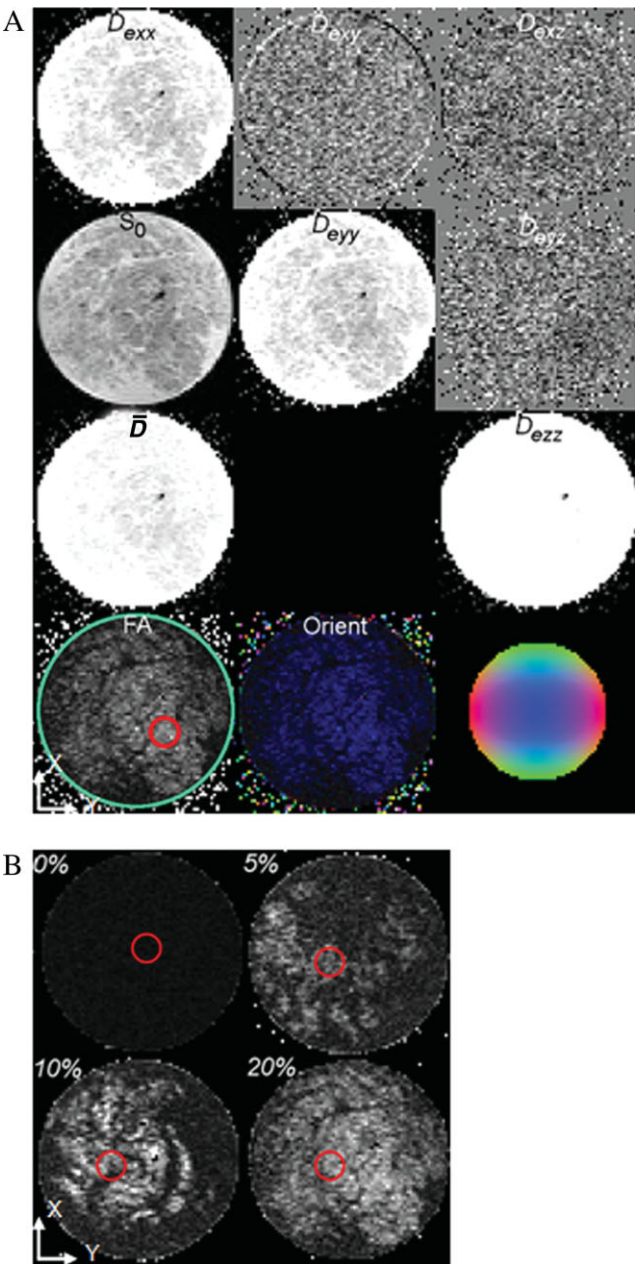

Figure 5 Diffusion tensor images of 1% hydrogels with various fiber contents obtained on a 14.1-T magnet system (field of view = 4.2 × 4.2 mm^2). (A) Sample with 20% fibers. The top row contains the $\boldsymbol{D}_e$ tensor element De_{ij} images D_{exx}, D_{exy}, and D_{exz} in gray scale. The second row contains the image without diffusion weighting (S_o) and the tensor elements D_{eyy} and D_{eyz}. The third row contains the mean diffusivity ($\bar{D}$) and D_{ezz}. The fourth row contains the FA image with the circular ROI used in Table I and an orientation map (Orient) image representing the directions of maximum diffusivity. The Orient image is colored according to the direction indicated by the color sphere on the right with the color intensity scaled by the FA. Blue represents the direction perpendicular to the image plane, green represents up and down, and red represents left to right. (B) FA images for samples with various fiber contents. Red circles correspond to the ROI used in Table I. [Color figure can be viewed in the online issue, which is available at www.interscience.wiley.com.]

TABLE I
Effective Diffusivity and FA of Water as Measured by DTI in 1% Hydrogel Samples Embedded with Glass Fibers

	Diffusivity in the entire sample								Diffusivity in an ROI							
	λ_z (cm^2/s)		λ_x (cm^2/s)		λ_y (cm^2/s)		FA		λ_z (cm^2/s)		λ_x (cm^2/s)		λ_y (cm^2/s)		FA	
Glass fiber (%)	Mean ($\times 10^{-7}$)	SD ($\times 10^{-9}$)	Mean ($\times 10^{-7}$)	SD ($\times 10^{-9}$)	Mean ($\times 10^{-7}$)	SD ($\times 10^{-9}$)	Mean	SD ($\times 10^{-3}$)	Mean ($\times 10^{-7}$)	SD ($\times 10^{-9}$)	Mean ($\times 10^{-7}$)	SD ($\times 10^{-9}$)	Mean ($\times 10^{-7}$)	SD ($\times 10^{-9}$)	Mean	SD ($\times 10^{-3}$)
0	2.13	2.64	1.98	3.23	1.88	0.35	0.064	6.45	2.13	0.76	1.97	0.98	1.88	0.84	0.065	1.69
5	2.17	0.75	1.93	0.45	1.80	0.69	0.098	2.69	2.19	0.84	1.77	1.45	1.64	1.31	0.16	4.94
10	2.16	0.75	1.85	0.83	1.73	1.01	0.12	2.34	2.16	1.15	1.65	1.63	1.52	1.53	0.2	6.50
20	2.29	2.62	1.89	1.87	1.75	2.04	0.15	1.96	2.31	1.14	1.71	1.07	1.58	1.21	0.21	3.82

Glass fiber (%)	$\lambda_z/\lambda_\perp$ [a]	$\lambda_z/\lambda_\perp$ [a]
0	1.10	1.10
5	1.16	1.28
10	1.20	1.36
20	1.26	1.40

Measures were over the entire sample and a local ROI (see Fig. 3).
[a] $\lambda_\perp$ was calculated as the average of λ_x and λ_y.

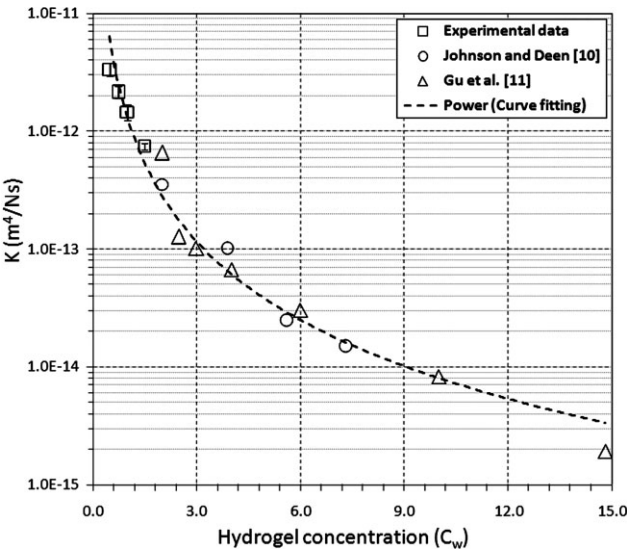

Figure 6 Measured hydraulic conductivity of fiber-free agarose hydrogels at low concentrations. Each □ data point is the average of four samples tested over a V range of 0.2–1.5 $\times$ 10^{-6} m/s. The bars correspond to ±1 SD. For reference, data from previous hydrogel studies by (△) Johnson and Deen[10] and (○) Gu et al.[11] are also graphed. The Darcy permeability in ref. 11 was converted to hydraulic conductivity through division by the water viscosity (μ = 0.001 N s/m^2). The power-law fit is given by K = 1.0 $\times$ $10^{-12}(C_w)^{-2.23}$ m^4 N^{-1} s^{-1} (where C_w = Weight of the hydrogel/Total water volume; R^2 = 0.9706).

free and 20% fiber samples, increases in fluid flow rates resulted in approximately linear increases in the pressure drop [Fig. 7(A)]. Measured pressure drops within 20% fiber samples were consistently greater than those within fiber-free samples. In all samples, there was greater variation in pressure responses (larger SD) with increasing flow rates. Corresponding hydraulic conductivities were not sensitive to changes in the flow rate in either type of sample over the flow range tested [Fig. 7(B)]. $K_\parallel$ in 20% fiber volume samples was slightly lower than that in other 1% hydrogel samples [Fig. 7(B) and Table II]. For example, $K_\parallel$ in 20% fiber volume samples

TABLE II
Permeameter-Measured Hydraulic Conductivities (K and $K_\parallel$) in the Tissue Surrogate

	w/v (%)	K (10^{-12} m^4 N^{-1} s^{-1})	SD (10^{-12} m^4 N^{-1} s^{-1})
Agarose hydrogel	0.5	3.35	0.401
	0.75	2.15	0.251
	1	1.47	0.225
	1.5	0.74	0.043
1% agarose hydrogel with glass fibers	5	1.46	0.159
	10	1.41	0.169
	20	1.20	0.079

Average values over the flow rate range of 10–50 μL/h (0.2–1.1 $\times$ 10^{-6} m/s) are presented.

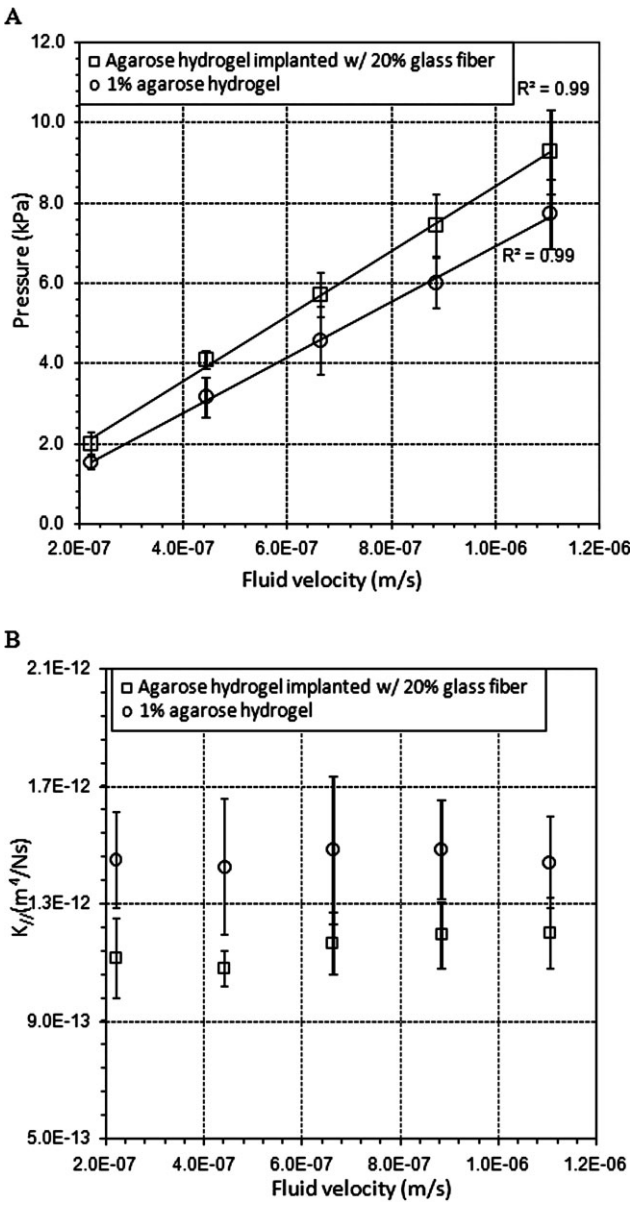

Figure 7 Effect of embedded glass fibers on K. (A) Measured pressure drop across the hydrogel samples versus V for fiber-free hydrogels ($n = 5$) and hydrogels implanted with glass fibers ($n = 4$). Linear curve fits are also plotted ($R^2 = 0.99$). (B) K versus V. $K = K_{\|}$ in the hydrogel with fibers. The bars correspond to ± 1 SD, and n is the number of samples tested.

was measured to be $1.20 \pm 0.22 \times 10^{-12}$ m^4 N^{-1} s^{-1}, which was approximately 18% lower than that in fiber-free samples. For other 1% hydrogel samples (0–10% fiber volume fractions), only small changes in $K_{\|}$ were measured (Table II).

Tracer infusion tests

EBA tracer distributions into fiber-free hydrogels were approximately spherical [Fig. 8(A)], and minimal backflow was observed. By the fitting of measured concentration profiles to numerical porous medium solutions [Fig. 9(A)], optimal ϕ and D values for the 1% hydrogel were estimated by minimization of the MSE value [Fig. 9(B)]. ϕ was estimated to be 0.6, and D was estimated to be 7.0×10^{-7} cm^2/s. As can be seen in the MSE map, numerical solutions were more sensitive to changes in ϕ than to changes in tracer diffusivity. This was likely due to the short times of tracer transport and/or the relatively high flow rates used in these experiments; that is, transport was not diffusion-dominated.

In the hydrogel samples with embedded fibers, EBA tracer distributions were approximately elliptical [Fig. 8(B)]. Ellipse ratios were found to increase nonlinearly with increasing fiber content (Table III). In these experiments, substantial backflow was observed in some infused samples; however, these samples were excluded from our analysis.

In a parameter sensitivity analysis, tracer transport in the porous medium model was simulated for

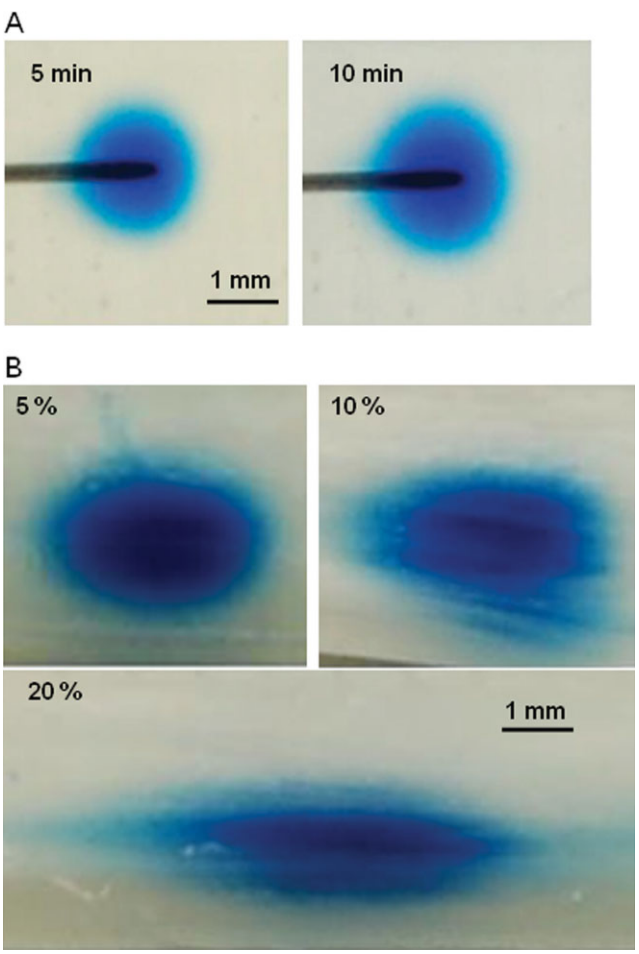

Figure 8 Images of the distribution of the EBA tracer into (A) fiber-free 1% hydrogel samples at various infusion times and (B) 1.0% hydrogel samples with various fiber contents at 20 min. The infusion flow rate was 10 μL/h. [Color figure can be viewed in the online issue, which is available at www.interscience.wiley.com.]

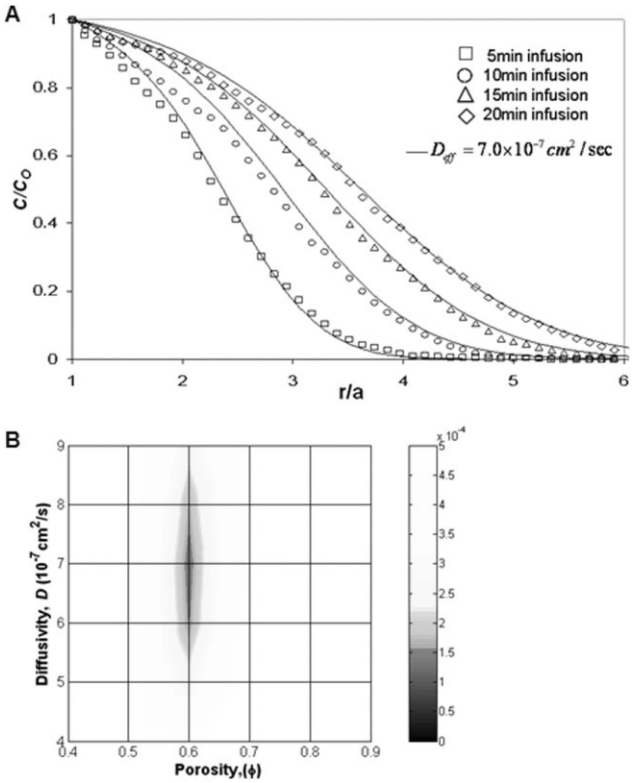

Figure 9 Diffusivity of EBA. (A) Experimental concentration profiles versus integrated concentration profiles for EBA infusions into 1.0% hydrogels. Average experimental (points) and computational concentration profiles (lines) are plotted with the distance from the infusion point. Simulated profiles use best fit parameters obtained by minimization of the MSE function. C/C_o is the normalized EBA concentration, and a is the outer diameter of the infusion cannula ($a = 0.25$ mm). (B) MSE map comparing the experimental EBA distribution data with numerical porous medium solutions. ϕ was estimated to be 0.6, and EBA diffusivity was estimated to be 7.0×10^{-7} cm^2/s for $1.0 < R/a < 6$.

various $K_{\|}/K_{\perp}$ ratios. The relationship between the predicted tracer ellipse ratio and $K_{\|}/K_{\perp}$ (with $K_{\|}$ kept fixed) is shown in Figure 10. Three lines are plotted for various fiber contents (5, 10, and 20%) with estimated transport properties. (Input ϕ values of 0.57, 0.54, and 0.48 were lower bound values based on the fiber volume and the baseline 1.0% hydrogel ϕ value of 0.6.) The ellipse ratio was found to change nonlinearly with $K_{\|}/K_{\perp}$. There were large changes in the ellipse ratio for small changes in the $K_{\|}/K_{\perp}$ ratio at low values of $K_{\|}/K_{\perp}$, and the ellipse ratio became less sensitive to changes as the magnitude of $K_{\|}/K_{\perp}$ increased. By a comparison of these simulation results with the experimentally measured ellipse ratios from EBA infusions (Table III), the ranges for $K_{\|}/K_{\perp}$, based on ± 1 SD, were estimated to be 3–5, 6–10, and 40–90 for 5, 10, and 20% volume fiber fractions, respectively.

TABLE III
Ellipse Ratios for the EBA Tracer Distributions in 1% Hydrogels with Various Volume Fractions of Glass Fibers

Fiber volume (%)	Ellipse ratio	
	Mean	SD
0	1.1	0.07
5	1.5	0.2
10	1.9	0.3
20	3.2	0.3

Distributions were for infusions of 3.3 μL (10 μL/h for 20 min).

DISCUSSION

A tissue surrogate was developed, consisting of agarose hydrogel and glass fibers. A variety of agarose hydrogel concentrations were tested, and a 1% concentration was selected for the majority of tests because of the ease of handling, overall stiffness, and minimal experimental backflow. With the inclusion of aligned glass fibers, anisotropic transport was due to bulk alignment, where transport in the direction perpendicular to fiber alignment was hindered because the fibers acted as obstacles, and transport in the direction parallel with fibers was not hindered. Thus, preferential hydrogel transport

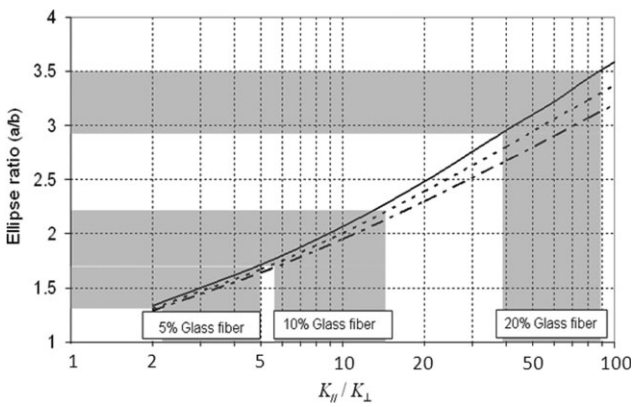

Figure 10 Numerical parameter analysis for EBA tracer transport in anisotropic porous media. The predicted EBA tracer distribution ellipse ratios versus hydraulic conductivity ratios ($K_{\|}/K_{\perp}$) were plotted after 20-min infusions (3.3 μL). Three cases were considered for glass-fiber volume fractions of (—) 20, (- - -) 10, and (– - –) 5% with estimated transport properties. (For the simulations, the properties for 20% fiber content were $K_{\|} = 1.20 \times 10^{-12}$ m^4 N^{-1} s^{-1}, $D_{\|} = 7.0 \times 10^{-7}$ cm^2/s, $D_{\|}/D_{\perp} = 1.26$, and $\phi = 0.48$. For 10% fiber content, the properties were $K_{\|} = 1.40 \times 10^{-12}$ m^4 N^{-1} s^{-1}, $D_{\|} = 7.0 \times 10^{-7}$ cm^2/s, $D_{\|}/D_{\perp} = 1.20$, and $\phi = 0.54$, and for 5% fiber content, the properties were $K_{\|} = 1.47 \times 10^{-12}$ m^4 N^{-1} s^{-1}, $D_{\|} = 7.0 \times 10^{-7}$ cm^2/s, $D_{\|}/D_{\perp} = 1.16$, and $\phi = 0.57$.) The horizontal gray bands correspond to the experimentally measured ellipse ratios $\pm$ 1 SD. The vertical gray bands provide the corresponding $K_{\|}/K_{\perp}$ ranges.

occurred in the direction parallel with fibers. Anisotropic transport was extensively characterized through DTI, pressure measurements, and tracer transport studies. The microscale composite structure was not quantified through imaging or microscopy studies because this is difficult to do at the resolution and under the hydrated conditions required.

With 5, 10, and 20% glass-fiber volume fractions, the tissue surrogate successfully provided preferential diffusional transport, as measured by DTI. The effective diffusivities for water were reduced in the transverse direction with the introduction of fibers that hindered diffusion. In the direction parallel to the fibers, the effective diffusivity was the same as that of the pure hydrogel. However, our surrogate had less diffusional anisotropy than in tissue. For example, in previous spinal cord DTI studies, the FA was determined to be between 0.67 and 0.87 in white matter regions.[22,23] This discrepancy is likely due to the relatively low glass-fiber volume fractions used in this study as well as the more uniform geometry of glass fibers compared with cellular structures. Also, the ϕ values of the hydrogel samples were estimated to be between 0.48 and 0.6, somewhat higher than the ϕ value of the extracellular space in nervous tissues, which is approximately 0.2.[24] By comparing tissue distributions of the albumin tracer to porous medium simulations, our group has previously estimated the $K_{\|}/K_{\perp}$ ratio in spinal cord tissues to be 16–20 for a 0.1 μL/min infusion.[16,25] This ratio is in the range estimated for this hydrogel surrogate.

In hydrogel-only samples, K was found to be highly sensitive to the water content. In this study, in comparison with previous studies by Johnson and Deen[10] and Gu et al.,[11] K was measured for lower hydrogel concentrations. However, the measured behavior of K, specifically the change in K with the hydrogel concentration, was consistent with the power-law behavior measured in these previous studies. In samples with fibers, the hydraulic conductivity in samples with 5 and 10% fiber contents did not differ greatly; however, for a 20% fiber volume fraction, $K_{\|}$ was lower in the direction parallel with the glass fibers in comparison with hydrogel-only samples. This may indicate that a threshold volume fraction may need to be reached before flow is hindered. Also, the measured hydraulic conductivities at a given fiber content were approximately constant and did not vary with the flow rate over the range tested.

Correspondingly, a rigid porous medium was considered for EBA transport simulations. For nonrigid media, the porous matrix structure is susceptible to deformation, which changes fluid transport properties, including hydraulic conductivity.[11] However, no clear changes in hydraulic conductivity were measured for the range of flow rates used in this study. This indicates that deformation did not have a large effect on transport and that a rigid medium model is reasonable. This contrasts with creep and dynamic loading studies by Gu et al.,[11] who estimated hydraulic permeability for agarose gels (no fibers) via fitting to biphasic solutions. They found K to be strongly dependent on the strain rate or hydrogel deformation. However, their creep and dynamic loading likely resulted in greater pore deformation than occurred in our study, in which pressures were low and significant deformation was not observed.

Transport anisotropy and increases in the measured $K_{\|}$ values could also be due to delamination or separation between the glass fibers and hydrogel interfaces. However, in our measurements, the hydraulic conductivity of the fiber-free hydrogels was higher than that of the hydrogels with 20% fiber content. This indicates that fluid flow was through the hydrogel space only, and separation was not a likely contributing factor at the low flow rates tested. If separation were an issue, the measured hydraulic conductivity of the hydrogel–fiber composite would be higher in the direction parallel to the fibers because the fluid would flow in separated regions more easily.

In EBA infusion studies, low volume fractions of fibers (<10%) did not result in extensive tracer transport anisotropy. However, transport anisotropy increased with the fiber content, especially with 20% fiber volume fractions. This behavior may indicate that a threshold fiber density is required before anisotropic fluid flow behavior becomes significant (e.g., flow is hindered in the plane perpendicular to fiber alignment). Through the use of tracer distribution data, the estimated ratio of directional hydraulic conductivity, $K_{\|}/K_{\perp}$, was determined to increase with the fiber content. The estimated ranges for $K_{\|}/K_{\perp}$ also increased with the fiber volume fraction increasing. These increases were due to the nonlinear relationship between the tracer distribution ellipse ratio and $K_{\|}/K_{\perp}$ (see Fig. 10). Thus, the larger range of $K_{\|}/K_{\perp}$ for samples with 20% fiber content was due to the lesser sensitivity of the tracer transport solutions to large values of $K_{\|}/K_{\perp}$. Such nonlinear behavior was expected because tissue transport is governed by coupled contributions of diffusion and convection. Convection, which is driven by a pressure gradient, is dominant near the infusion site, where the decay in the pressure is steepest and the velocities are greatest. With increasing distance from the infusion site, the contribution by diffusion to transport increases, and this results in nonlinear behavior. For the infusion volumes and flow rates studied, convection and diffusion were of the same order.

The Peclet number (*Pe*), which is the ratio of the characteristic time of diffusion (t_d) to the characteristic time of convection (t_c; $Pe = t_d/t_c$), was calculated to compare the relative contributions of convection and diffusion to EBA tracer transport. Transport is diffusion-dominated for small *Pe* values ($\sim$ 1 or less) and convection-dominated for large *Pe* values ($\sim$ 10 or more). t_d is given by $t_d = (\bar{r})^2/D_{\text{eff}}$, where D_{eff} is the effective tracer diffusivity and $(\bar{r})$is the characteristic length. t_c is described by $t_c = \int_a^{\bar{r}} dr/v(r)$. *Pe* for a constant flow rate infusion was calculated as follows[26]:

$$Pe = \frac{3Q\bar{r}^2}{4\pi D_{\text{eff}}(\bar{r}^3 - a^3)}$$

where Q is the infusion flow rate. For a constant infusion of EBA at 3.33 μL/h, *Pe* for the hydrogel was 7.6 when D_{eff} was 7.0×10^{-5} mm^2/s, a was 0.25 mm, Q was 10 μL/h, and $\bar{r}$ was 1 mm. This analysis also shows convection and diffusion to be of the same order.

CONCLUSIONS

In the fabrication of these fiber-embedded hydrogels, care must be taken to minimize air bubble formation and provide an even distribution of fibers. An experimental source of error that contributed to variation in the measured $K_{\parallel}$ values and ellipse ratios was likely the nonuniformity of the distributed glass fibers in the hydrogel; however, the bulk of the fibers appeared to be aligned. Overall, the developed hydrogel model was able to provide a uniform, anisotropic test medium suitable for low-flow-rate infusion studies. At higher infusion rates, backflow as well as weak connectivity between the hydrogel and glass fibers may be introduced. We expect that the developed hydrogel model can be used for *in vitro* transport studies to mimic the extracellular transport of anisotropic tissues, and measurements of hydraulic conductivity are useful for the analysis of convective transport. In future studies, the fabrication methodology may be modified for various applications. For example, hydrogel properties, such as the polymer size and crosslinker concentration, may be altered.[17] Also, glass fibers were chosen to provide an underlying aligned structure. However, they do not have the biodegradability of some polymers. In future studies, fibers of alternate compositions may be substituted.

The authors thank Roger Tran-Son-Tay and Bhavani Shankar for providing testing facilities, equipment, and materials. They also thank Daisy Evans and Prinda Wanakule for aiding with the experimental studies. The MR imaging data were obtained at the Advanced Magnetic Resonance Imaging and Spectroscopy Facility of the McKnight Brain Institute and at the National High Magnetic Field Laboratory of the University of Florida.

References

1. Drury, J. L.; Mooney, D. J. Biomaterials 2003, 24, 4337.
2. Suh, J. K. F.; Matthew, H. W. T. Biomaterials 2000, 21, 2589.
3. Lee, C. H.; Singla, A.; Lee, Y. Int J Pharm 2001, 221, 1.
4. Bobo, R. H.; Laske, D. W.; Akbasak, A.; Morrison, P. F.; Dedrick, R. L.; Oldfield, E. H. Proc Natl Acad Sci 1994, 91, 2076.
5. Lonser, R. R.; Gogate, N.; Morrison, P. F.; Wood, J. D.; Oldfield, E. H. J Neurosurg 1998, 89, 610.
6. Prokopova, S.; Vargova, L.; Sykova, E. NeuroReport 1997, 8, 3527.
7. Tao, L.; Nicholson, C. Neuroscience 1996, 75, 839.
8. Liang, S. M.; Xu, J.; Weng, L. H.; Dai, H. J.; Zhang, X. L.; Zhang, L. N. J Controlled Release 2006, 115, 189.
9. Buschmann, M. D.; Gluzband, Y. A.; Grodzinsky, A. J.; Hunziker, E. B. J Cell Sci 1995, 108, 1497.
10. Johnson, E. M.; Deen, W. M. AIChE J 1996, 42, 1220.
11. Gu, W. Y.; Yao, H.; Huang, C. Y.; Cheung, H. S. J Biomech 2003, 36, 593.
12. Huang, Z.; Zhang, Y. Z.; Kotaki, M.; Ramakrishna, S. Compos Sci Technol 2003, 63, 2223.
13. Subbiah, T.; Bhat, G. S.; Tock, R. W.; Parameswaran, S.; Ramkumar, S. S. J Appl Polym Sci 2005, 96, 557.
14. Small, W. R.; Paunov, V. N. J Mater Chem 2008, 18, 2082.
15. Green, N. G.; Morgan, H. J Phys D: Appl Phys 1997, 30, 2626.
16. Yamamoto, I.; Ozawa, S.; Makino, T.; Yamaguchi, M.; Takamasu, T. Sci Technol Adv Mater 2008, 9, 024214.
17. Gillies, G. T.; Wilhelm, T. D.; Humphrey, J. A. C.; Fillmore, H. L.; Holloway, K. L.; Broaddus, W. C. Nanotechnology 2002, 13, 587.
18. Basser, P. J.; Mattiello, J.; Lebihan, D. Biophys J 1994, 66, 259.
19. Chen, X. M.; Sarntinoranont, M. Ann Biomed Eng 2007, 35, 2145.
20. Chen, X.; Astary, G. W.; Sepulveda, H.; Mareci, T. H.; Sarntinoranont, M. Magn Reson Imaging 2008, 26, 1433.
21. Schenck, J. F. Med Phys 1996, 23, 815.
22. Gullapalli, J.; Krejza, J.; Schwartz, E. D. J Magn Reson Imaging 2006, 24, 231.
23. Sarntinoranont, M.; Chen, X. M.; Zhao, J. B.; Mareci, T. H. Ann Biomed Eng 2006, 34, 1304.
24. Nicholson, C.; Sykova, E. Trends Neurosci 1998, 21, 207.
25. Sarntinoranont, M.; Banerjee, R. K.; Lonser, R. R.; Morrison, P. F. Ann Biomed Eng 2003, 31, 448.
26. Netti, P. A.; Travascio, F.; Jain, R. K. AIChE J 2003, 49, 1580.